Visual Abstract

Fatigue growth rate of inclined surface cracks in aluminum and titanium alloys

R.R. Yarullin, M.M. Yakovlev
Institute of Power Engineering and Advanced Technologies FRC Kazan Scientific Center of RAS, Russia
yarullin_r@mail.ru, yakovlev.mikhail.m@yandex.ru

ABSTRACT. In this paper the fatigue crack growth tests were carried out on surface-crack tension (SCT) specimens, made of 7050 and Ti6Al4V alloys, with initial semi-elliptical surface cracks. Pure Mode I conditions were realized on SCT specimens with crack plane located orthogonal to the loading direction, while Mixed-mode conditions were observed on SCT specimens with inclined crack. Optical microscope measurements and the crack mouth opening displacement (CMOD) method were respectively used to monitor crack length and calculate crack depth. Current crack shape during the tests was highlighted by alternation of loading spectrum with baseline load block and a marker load block. The stress strain field along the crack front of semi-elliptical cracks in the SCT specimens was assessed by Finite Element Method (FEM) analysis. The stress intensity factors (SIFs) were calculated along crack fronts and equivalent elastic SIF formulation was used for crack growth rate assessment under mixed mode conditions. As a result, the fracture resistance parameters of aluminum and titanium alloys were obtained for two crack propagation directions under Mode I and Mixed-mode loading. The benefits of using the computational and experimental results of SCT specimen for the assessment of the surface crack growth rate in aluminum and titanium alloys under Mixed-mode loading conditions were stated.

KEYWORDS. Inclined surface cracks; Fatigue crack growth; Mixed-mode conditions; Aluminum alloy; Titanium alloy.

Citation: Yarullin, R.R., Yakovlev, M.M, Fatigue growth rate of inclined surface cracks in aluminum and titanium alloys, Frattura ed Integrità Strutturale, 60 (2022) 451-463.

Received: 28.02.2022
Accepted: 18.03.2022
Online first: 21.03.2022
Published: 01.04.2022

INTRODUCTION

Surface cracks are typical damages in aircraft structure components, and their growth can lead to catastrophic failures. In service, fatigue surface cracks were found to grow in turbine disks, high-pressure compressor disks, turbine blades, load-carrying components of a frame structures, levers and the airplanes' landing-gear components [1]. A surface flaws feature is that the crack grows simultaneously in two directions and changes its shape from initial i.e. related to the defect nature (risk, pore, pothole) to final i.e. at fracture. At the same time, a significant crack growth rate reduction in the

deepest point of the crack front with respect to the crack front intersection with the free surface of the tested specimens can be observed as a function of loading conditions [2].
Although some surface cracks in structural components are subjected to uniaxial or Mode I loading type, in most cases the loading direction and the operational damage plane are not perpendicular to each other and such defects are considered as inclined cracks [3]. The elastic–plastic stress fields and mode mixity parameters for semi-elliptical surface cracks on biaxial loaded plates have been investigated in [4] using detailed three-dimensional finite element calculations. Different degrees of mode mixity are given by combinations of the far-field stress level, biaxial stress ratio and inclined crack angle. Normalized mixed-mode stress intensity factor equations were presented in the paper [5] for deflected and inclined circular surface and corner cracks in finite-thickness plates under uniform tensile loads. In the resulting equations, different deflection and inclination crack angles were considered, and plate thickness effects were included.
However, at present time, there are no fracture resistance parameters for materials under Mixed-mode loading conditions for defects with initial shape close to operational damages. In this paper, the computational and experimental results for inclined surface cracks in SCT specimens of aluminum and titanium alloys are provided for Mixed-mode loading conditions. The fracture resistance parameters for inclined surface cracks and their comparisons with results available in the literature are presented.

SUBJECT OF THE STUDY, MATERIAL PROPERTIES, AND EXPERIMENTAL CRACK PATHS

The subject of this study is surface-crack tension (SCT) specimens of aluminum and titanium alloys. The plates with surface cracks as well as the modified ASTM E740 [6] SCT specimens with inclined surface crack are widely used for the Mixed-mode fatigue growth under tension and bending loading [7-10].
The SCT specimens' thickness B is equal to 10 mm, the specimen's width W is equal to 40 mm, and the specimen's length L is equal to 56 mm. The SCT specimens with starter notch a_0=2 mm, c_0=2 mm and initial inclined plane α=0° are used for pure Mode I loading conditions (Fig. 1a). The SCT specimens with starter notch a_0=2 mm, c_0=2 mm and initial inclined plane α≈30°-45° are used to provide 3D Mixed-mode problems (Fig. 1b).

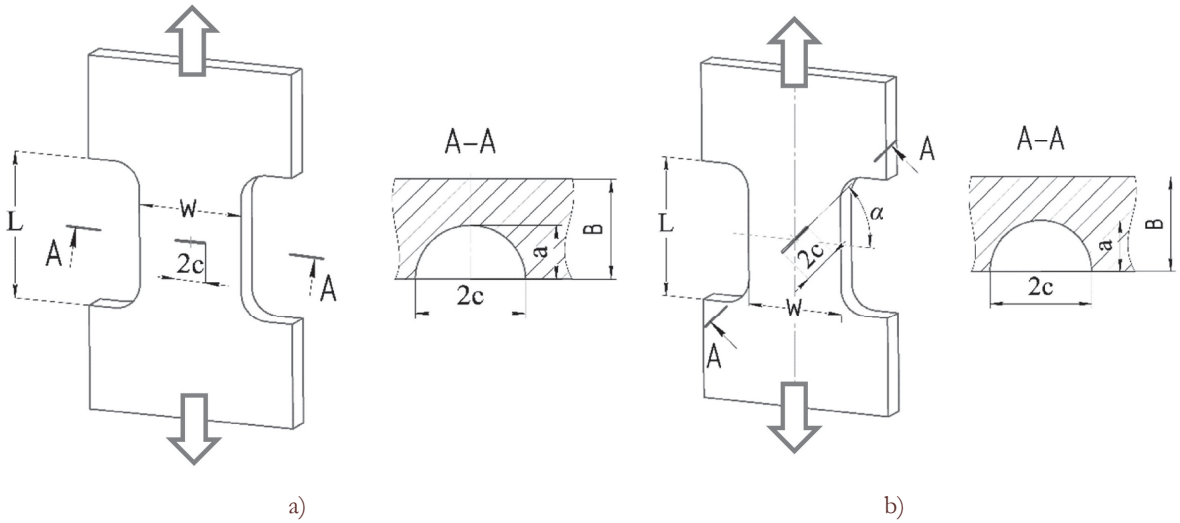

a) b)

Figure 1: SCT specimen geometry for pure Mode I (a) and Mixed Mode loading (b).

A typical aerospace material, 7050 aluminum and Ti6Al4V titanium, were chosen for the experiments due to its extended use in industrial applications. 7050 aluminum possesses high specific strength and stiffness, excellent fabricability and low cost. The Ti6Al4V titanium is applied in the aeronautical industry due to high specific mechanical strength, fracture toughness, fatigue strength and high temperature stability. The SCT specimens were taken from rolled aluminum and titanium alloys such that longitudinal (L) grain direction would be under investigations.
The tensile properties of considered alloys at room temperature were determined according to the ASTM standard E8 and are listed in Table 1: σ_0 is the monotonic tensile yield strength, σ_s is the nominal ultimate tensile strength, σ_u is the true

ultimate tensile strength, α is the strain hardening coefficient, *n* is the strain hardening exponent, *E* is the Young's modulus, δ is the elongation and ψ is the reduction of area.

Material	σ_0, MPa	σ_S, MPa	σ_u, MPa	α	n	E, GPa	δ, %	ψ, %
7050	472	524	701	1.570	10.85	70.57	11	28
Ti6Al4V	886	964	1290	1.225	12.59	118.00	16	29

Table 1: Main mechanical properties of aluminum and titanium alloys at room temperature.

Fatigue precracking of SCT specimens was performed under three-point bending mode according to the method described in [6]. SCT specimen with starter notch plane α=30°-45° was turned relative to test tool set in order to obtain Mode I conditions at notch tip (Fig. 2). Precracking was completed when the crack length *c* reached 4.5-5.0 mm. The nominal stresses magnitude during fatigue precracking was such to not exceed material yield strength and was equal to 157.5 MPa.

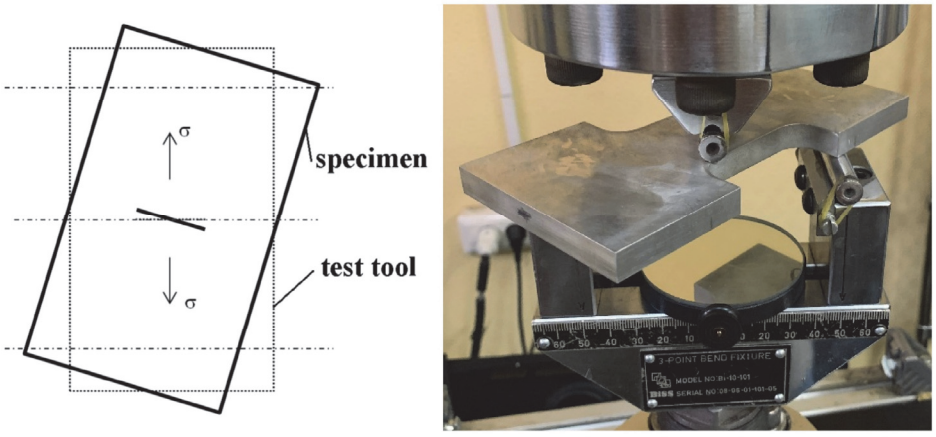

Figure 2: Fatigue precracking procedure for SCT Mixed-mode loading specimen.

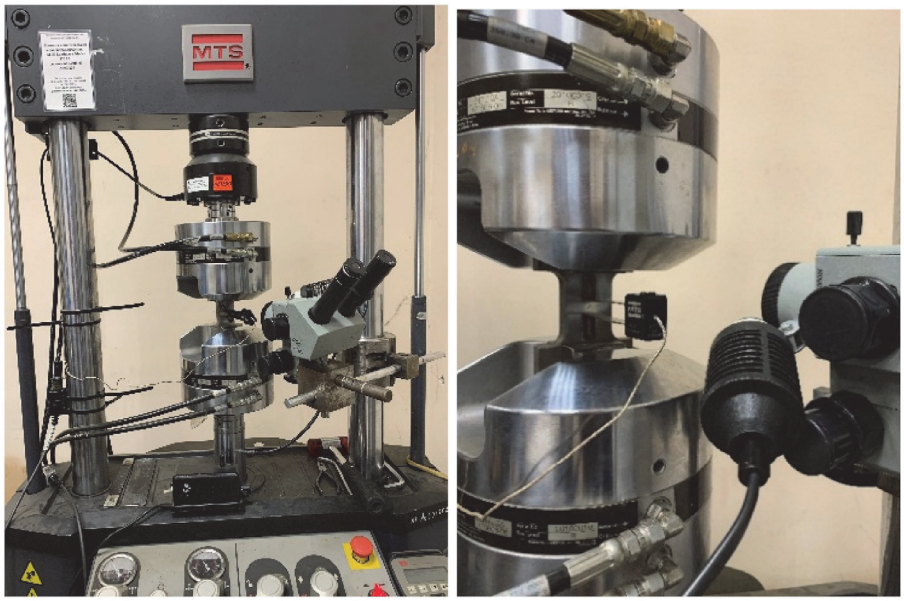

Figure 3: Test equipment for SCT specimens fatigue crack growth tests.

The SCT specimens fatigue crack growth (FCG) tests are carried out on an MTS Landmark servo-hydraulic test system with a maximum capacity of 100 kN at 10 Hz frequency and with R_s=0.1 stress ratio (Fig. 3).
The Mode I and Mixed-mode tests of the 7050 and Ti6Al4V SCT specimens were performed by applying uniaxial forces *P=42 kN* and *P=60 kN*, respectively. All tests were carried out with sinusoidal loading. Load control was estimated to be better than ±1%. The crack length on the specimen's free surface was monitored using an optical microscope. Crack mouth opening displacement (CMOD) measurements was used for crack depth determination. The displacement gage length was equal to 10 mm. For SCT Mixed-mode specimen the CMOD device was placed in the load application direction (Fig. 3).
Two different stress ratio values (0.1 and 0.5) were applied several times to each SCT specimen in order to fix the current crack front position. During each test, beach marks were produced for each SCT specimen by increasing the applied stress ratio from 0.1 to 0.5 at a constant value of the maximum cyclic nominal stress, while the surface crack length was increased by approximately 0.1-0.2 mm. As shown in [11-13], the beach mark loading does not induce load history effects or overload retardation. The typical fracture surface marks are shown in Fig. 4a and 4b for SCT Mode I and SCT Mixed-mode specimens, respectively.

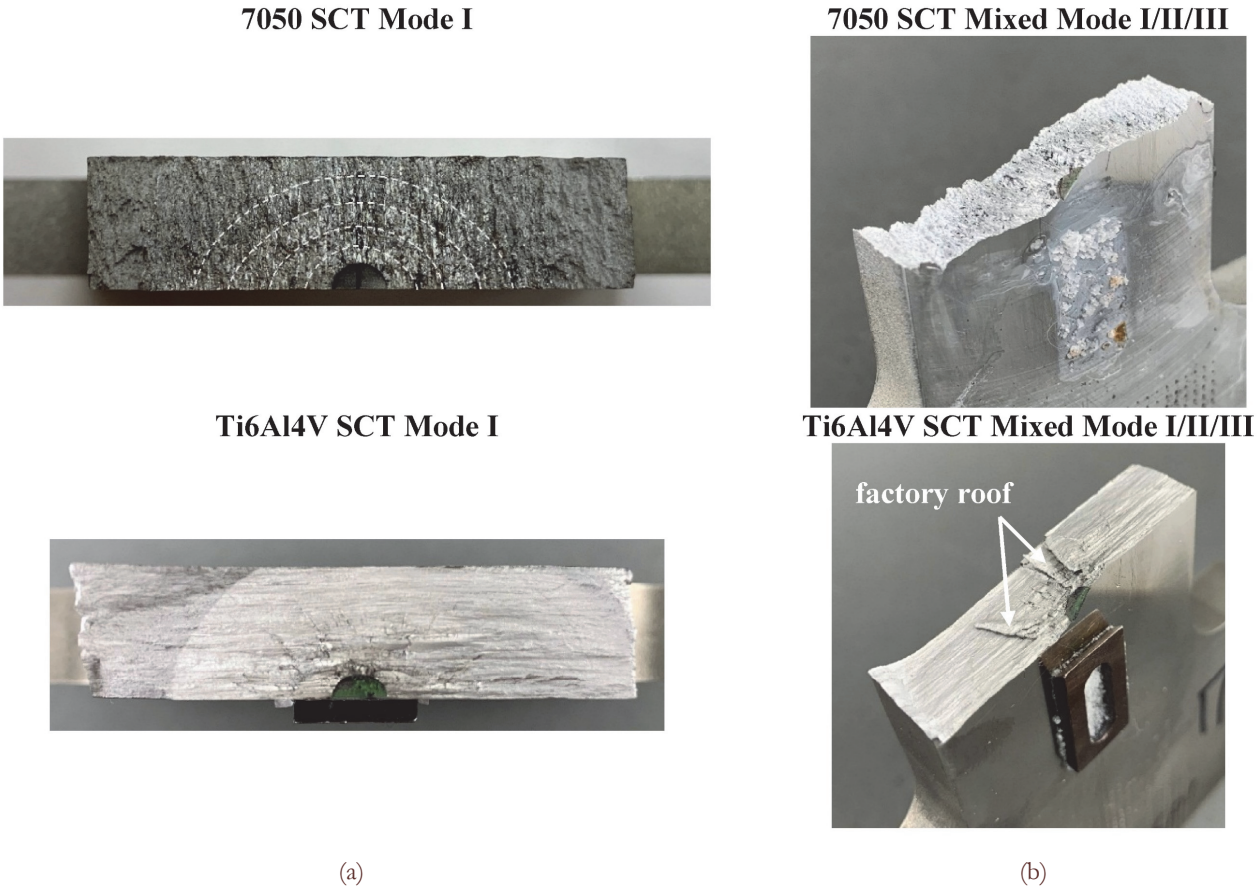

Figure 4: Fracture surfaces for (a) Mode I and (b) Mixed-mode loading.

Factory roof patterns were found on fracture surface of SCT Mixed-mode specimen from titanium alloy. Factory-roofs initiate by elementary Mode I branches at particular sites on the fronts of semi-elliptical surface cracks growing under Mixed-mode II + III [14]. The factory roof patterns' roughness (or visibility) particularly depends on the applied cyclic shear stress amplitude and also the material microstructure significant influence. These conditions, along with the material yield strength, constitute the main reasons why the factory roof patterns are not observed in the 7050 aluminum alloy.
From the crack front shape obtained by beach mark procedure, the crack length measurements c on the free surface (width/height direction) and the crack depth a of growing surface crack (thickness direction) can be obtained for SCT specimens using an optical instrumental microscope. The experimental crack sizes combinations for SCT Mode I and Mixed-mode specimens for aluminum and titanium alloys are presented in Table 2.

Materials	Mode I Surface crack sizes a/c (mm/mm)				Mixed-mode Surface crack sizes a/c (mm/mm)		
	1st front	2nd front	3rd front	4th front	1st front	2nd front	3rd front
7050	3.19/5.00	4.32/6.27	6.19/8.51	-	2.53/4.55	4.47/7.25	7.70/12.50
Ti6Al4V	2.50/5.08	4.10/6.18	5.90/7.73	7.75/9.73	2.50/4.65	4.00/6.70	7.70/13.00

Table 2: Experimental crack sizes for SCT specimens.

For SCT Mixed-mode specimens the crack length *c* was measured along the curvilinear crack path on the specimen free surface, the crack depth *a* was measured on a plane orthogonal to the specimen's axis (Fig. 1b).
The fracture surface of SCT Mixed-mode specimens, as shown in Fig. 4b, illustrate the tortuous path the crack propagated through the microstructure. The curvilinear shape and orientation of the growing crack need to be modeled based on FEM methodology, which is not simple. This assumption was made because the tortuous crack path did not facilitate direct crack inclination angle measurements from the fracture surface. An alternative way is to do the initial inclination angle measurements (after precracking, Fig. 5a) and final inclination angle on the back side of the specimen (after fracture, Fig. 5b). Based on the crack plane inclination angle α performance along SCT Mixed-mode specimens thickness (Fig. 5c) it is possible to calculate the inclination angle for any experimental crack fronts. It is clear that while the crack, in its initial configuration, starts out as a Mixed-mode crack, after a substantial growth, the crack configuration is in a near pure Mode I state.

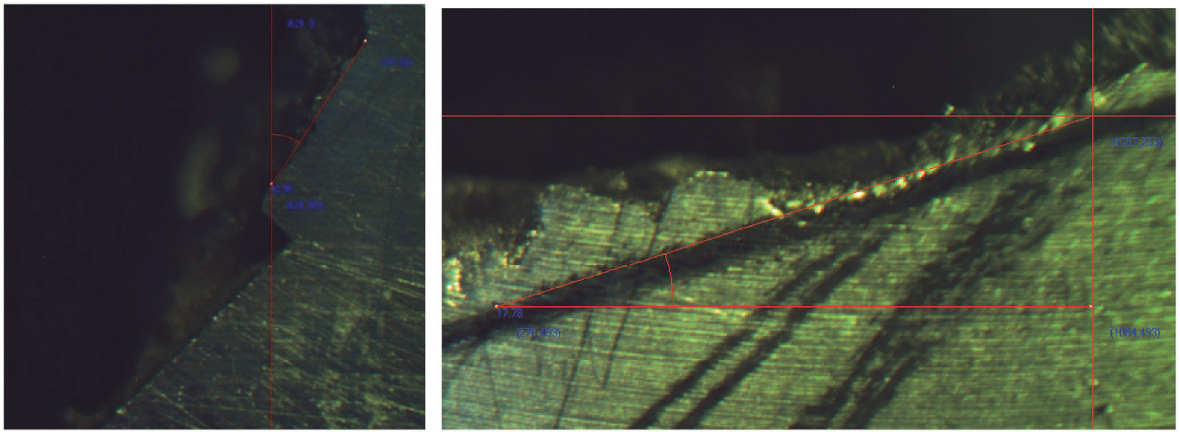

(a) (b)

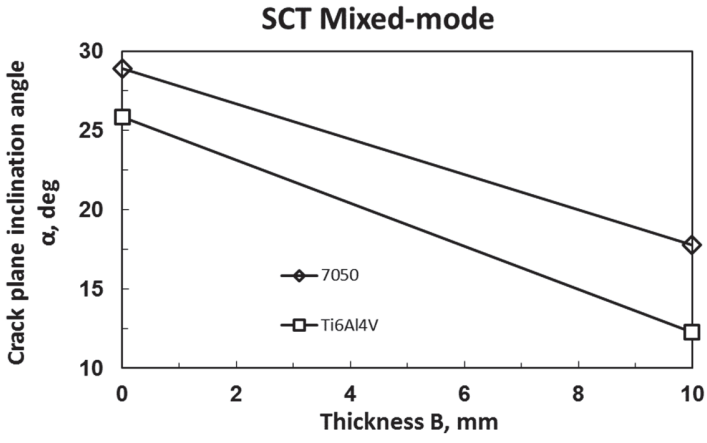

(c)

Figure 5: Crack plane inclination angle α (a) on the front side, (b) on the back side and (c) behavior along thickness of SCT Mixed-mode specimens.

As mentioned above, crack growth was monitored using the optical microscope and CMOD for Mode I and Mixed mode loading conditions on SCT specimens' tests. The relationships between CMOD and crack length on the free surface for both considered alloys under different loading conditions are plotted in Fig. 6. A strong correlation was found between these two parameters, and this information can be very useful for the crack growth rate diagram's interpretation in thickness direction.
Thus, the obtained experimental data of the crack front shape and orientation for various fatigue failure process stages will be used in this study to calculation the fracture parameters distributions along the crack fronts in terms of elastic and equivalent SIFs for all tested SCT specimens.

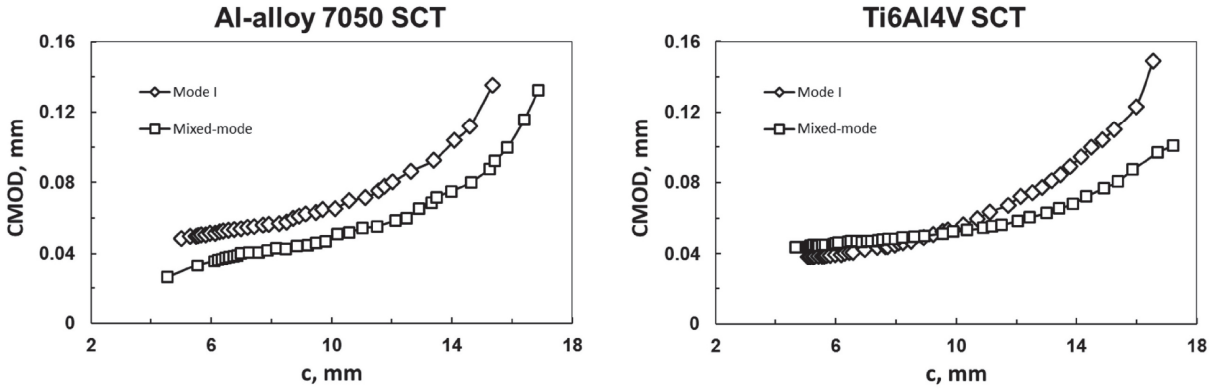

(a) (b)

Figure 6: Relationship between CMOD and crack length on the free SCT specimen surface for (a) aluminium and (b) titanium alloys under different loading conditions.

MIXED MODE CRACK GROWTH PARAMETERS

Equivalent stress intensity factor

3D Mixed Mode problems are characterized by the fracture superposition Modes I, II and III. While an existing crack under Mode I loading conditions will propagate within the original crack plane, Mode II loading generally leads to a crack kinking, Mode III loading causes the crack front twisting, for 3D Mixed Mode cases depending on the Mode II- and Mode III-portions a more or less intense crack deflection or crack twisting can be observed. This means, that within the linear-elastic fracture mechanics scope the SIFs K_I, K_{II} and K_{III} are of importance for the fracture risk estimation in structures as well as for the stable crack propagation evaluation processes [15] and can be defined by Eq. (1):

$$K_I = \sigma_y \sqrt{\pi a} \cdot Y_I \, , K_{II} = \tau_{xy} \sqrt{\pi a} \cdot Y_{II} \, , K_{III} = \tau_{yz} \sqrt{\pi a} \cdot Y_{III} \tag{1}$$

In general, the SIF depends on the stress (σ_y, τ_{xy} or τ_{yz}), the crack length *a,* and on the boundary correction factors (Y_I, Y_{II} or Y_{III}).
Shlyannikov [16] generalized the numerical method to calculate the geometry dependent correction factors Y_I, $Y_{II,}$ and Y_{III} for the SIFs K_I, K_{II}, and K_{III} under mixed mode fracture. The present study explores the direct use of FE solution results for calculating the SIFs K_I, K_{II}, $K_{III,}$ ahead of the crack tip (θ=0°):

$$K_I = \sigma_{\theta\theta}^{FEM} \sqrt{2\pi r} \, , K_{II} = \sigma_{r\theta}^{FEM} \sqrt{2\pi r} \, , \; K_{III} = \sigma_{\theta\omega}^{FEM} \sqrt{2\pi r} \tag{2}$$

where *r, θ,* and ω are polar coordinates centered at the crack tip, and σ_i^{FEM} are the stresses obtained from the FE solution.
To describe the Mixed-mode crack growth along the curvilinear crack path the equivalent elastic SIF includes Mixed-mode effects such that

$$K_{eqv} = \sqrt{\left(1-\nu^2\right)\left(K_I^2 + K_{II}^2\right) + \left(1+\nu\right)K_{III}^2} \tag{3}$$

was obtained from the energy release rate G definition for plane strain [17]:

$$G = G_1 + G_2 + G_3 = \frac{1-\nu^2}{E}\left(K_I^2 + K_{II}^2 + \frac{K_{III}^2}{1-\nu}\right) \tag{4}$$

where E is the Young's modulus, ν is the Poisson's ratio.

NUMERICAL STUDY

Elastic–plastic stress–strain fields along the crack front

The numerical calculations in this study are connected with the stress-strain state (SSS) SCT specimens' analysis with Mode I and inclined surface cracks. The ANSYS FE code [18] is used in the mechanical analysis. Twenty nodal solid brick elements with quadratic interpolation were used to mesh the 3D FE model configurations, which is a quarter of the SCT Mode I specimen and full geometry of the SCT Mixed-mode specimen. The FE models of SCT specimens were loaded with forces which coincides with the maximum experimental loads value and are *P=42 kN* and *P=60 kN* for 7050 and Ti6Al4V alloys, respectively. In order to perform numerical calculations, the main mechanical properties listed in Table 1 were used.

The crack tip shapes obtained by beach mark procedure has been considered in the numerical part of the study. The crack sizes for both alloys are presented in Table 2 and the crack inclination angles for SCT Mixed-mode specimens have been defined consistently from the Fig. 5c. As a result, for each considered material type, from 6 to 7 3D FE models with different crack front positions were analyzed under experimental loading conditions.

The SIFs were calculated using the topology building principles of FE meshes, the elements sizes, and their distribution density in the radial and circumferential directions, as applied to surface defects in real structures, components and specimens, which are described in [2, 4, 9, 19-21]. Thus, in order to accurately characterizing the influence of the strain gradient, a very refined mesh is used near the crack tip, where the elements' size is in the one micrometer order. The nodes number in the 3D FE models were varied from 1 000 000 to 2 500 000. Typical FE meshes for the SCT Mode I and SCT Mixed-mode specimens with surface crack are illustrated in Fig. 7a,b and 8a,b, respectively.

The typical equivalent stress distributions for the SCT Mode I and SCT Mixed-mode specimens with surface crack are illustrated in Fig. 7c and 8c, respectively.

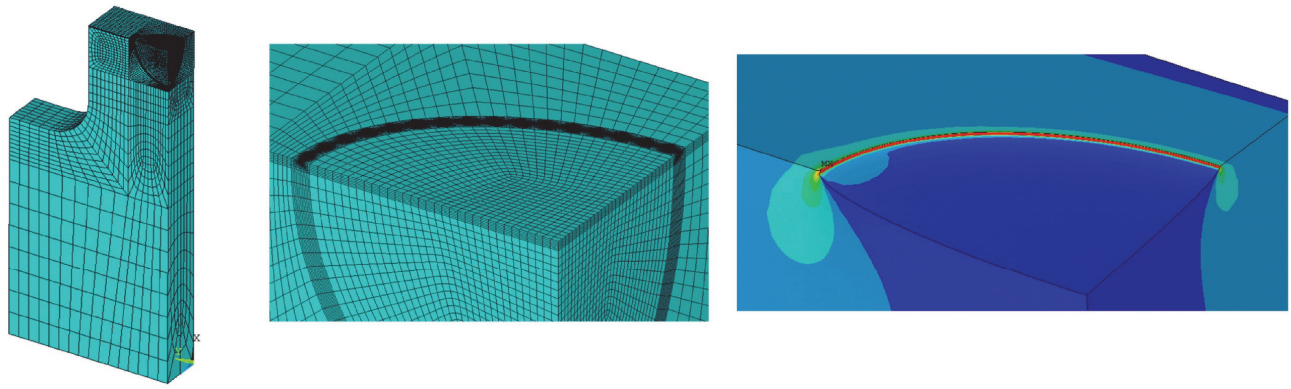

(a) (b) (c)

Figure 7: Typical (a, b) FE meshes and (c) equivalent stress distributions for SCT Mode I specimen with surface crack.

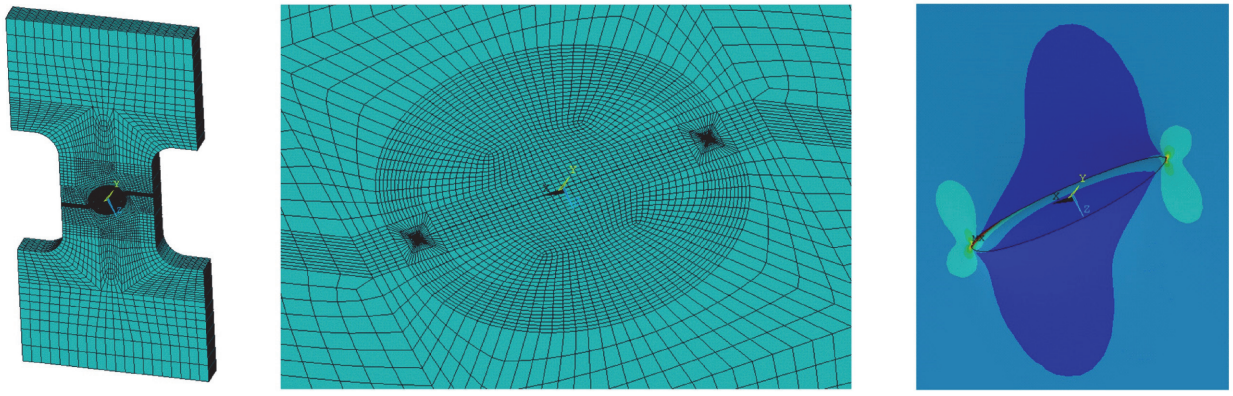

(a) (b) (c)

Figure 8: Typical (a, b) FE meshes and (c) equivalent stress distributions for SCT Mixed Mode specimen with surface inclined crack.

Stress intensity factors distributions

One of the main objectives of the present study is the elastic fracture mechanical parameters calculation for real shape and surface cracks sizes, which were obtained by uniaxial tension tests on two SCT specimens types. It should be recalled that the SCT specimens with crack plane located orthogonal to the loading direction was used to realize pure Mode I loading conditions, and the SCT specimens with inclined crack was proposed in order to reproduce the Mixed-mode loading conditions around the crack tip. The elastic SIFs K_I, K_{II} and K_{III} distributions and elastic equivalent Mixed-mode SIFs K_{eqv} were obtained by Eq. (2) and Eq. (3), respectively. All parameters are determined at the crack tip distance range r/a=0.0025-0.01, where the numerical solution provides a stabilized result. To compare the parameter distributions along surface crack tip, it is convenient to introduce dimensionless coordinates in the following form:

$$x_0 = \Delta\varphi\cos\varphi_0,\ y_0 = \Delta\varphi\sin\varphi_0,\ x_c = \Delta\varphi\cos\varphi_c,\ y_c = \Delta\varphi\sin\varphi_c,\ x_i = \Delta\varphi\cos\varphi_i,\ y_i = \Delta\varphi\sin\varphi_i,$$
$$\varphi_i \in [\varphi_0, \varphi_c], \Delta\varphi = \varphi_c - \varphi_0 \tag{5}$$

$$\bar{X}_i = \frac{x_0 - x_i}{x_0 - x_c}, \bar{Y}_i = \frac{y_i - y_0}{y_c - y_0},\ R_i = \frac{1}{\sqrt{2}}\sqrt{\bar{X}_i^2 + Y_i^2}, R \in [0,1] \tag{6}$$

where ϕ_0 is the angle determining the crack tip initial point position, and ϕ_c is the angle corresponding to the crack tip last point.

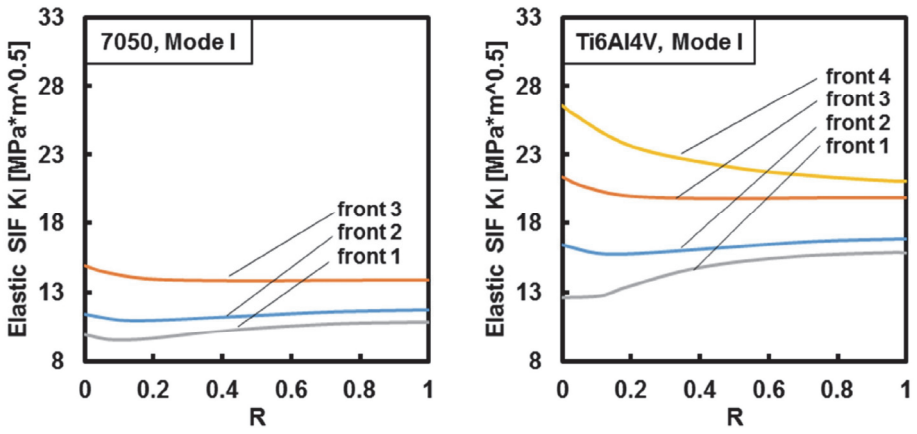

(a) (b)

Figure 9: Distributions of the elastic SIFs along the crack fronts for (a) aluminum and (b) titanium alloys under model I.

In the following numerical results representation, the authors will use the variable R in the 0 to 1. R=0 indicates the SCT specimens exterior free surface (c direction, Fig. 1), while R=1 indicates the crack tip deepest point (a direction, Fig. 1).
The SIFs K_I distributions along several crack fronts for both alloys at pure uniaxial tension loading conditions are plotted in Fig. 9. K_{II} and K_{III} are nearly zero during all crack fronts (consequently, K_{eqv} and K_I values nearly coincide), therefore were not reported.
Looking at this figure, it can be noted that the elastic SIFs K_I for the SCT Model I specimens are changed by a moderate amount in the range of $0<R<1$. Insignificant changes of the elastic SIFs K_I distributions are observed for front 4 in titanium alloy, which related to thickness effects.
The SIFs K_I, K_{II} and K_{III} distributions along several crack fronts for aluminium and titanium alloys at Mixed-mode loading conditions are plotted in Fig. 10 and Fig. 11, respectively. It is possible to note, that at approximately the same crack sizes and the same maximum load magnitude the SIF K_I values for Mode I loading conditions are insignificantly lower compared with SIF K_I for Mixed-mode, while the SIFs K_{II} values and K_{III} are nonzero. As expected, the SIFs K_{II} maximum values are observed on the SCT specimens' free surface; on the contrary to this the SIFs K_{III} maximum values are observed on the crack front deepest point. It shows that Mixed-mode loading conditions are realized for SCT specimens with initial inclination angle $\alpha \approx 25°$-$30°$. It should be note, that K_I keeps increasing trends while K_{II} and K_{III} are stabilized during the crack growth. It confirms that this Mixed-mode crack becomes the Mode I dominated one while growing.

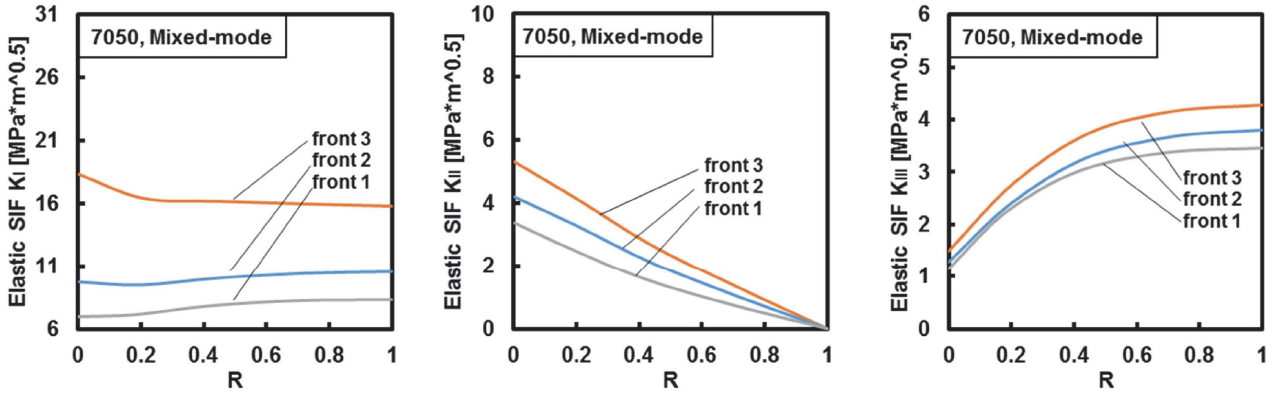

Figure 10: Elastic SIFs (a) K_I, (b) K_{II} and (c) K_{III} distributions along the crack fronts for aluminum alloy under Mixed-mode.

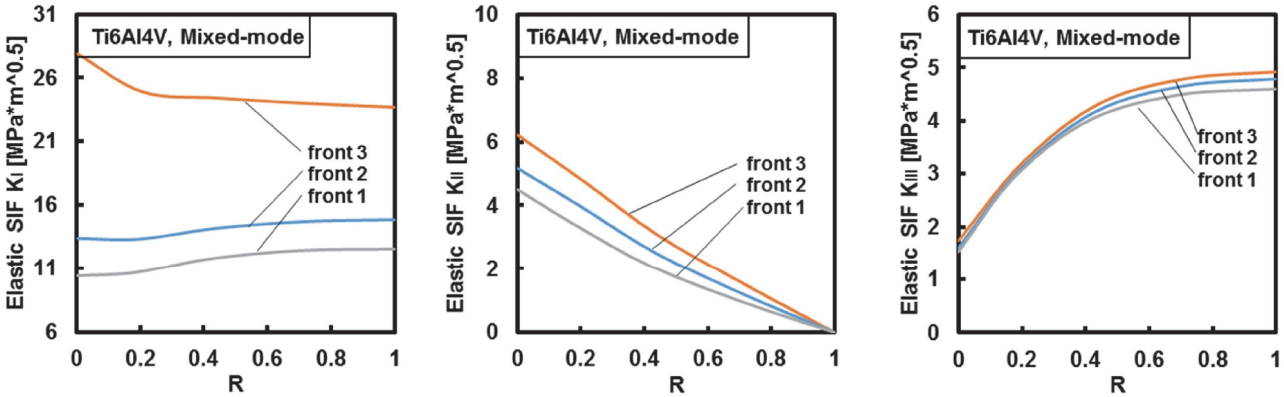

Figure 11: Elastic SIFs (a) K_I, (b) K_{II} and (c) K_{III} distributions along the crack fronts for titanium alloy under Mixed-mode..

The elastic SIFs K_{eqv} behaviors in the thickness direction and along the free surface (width/height direction) of growing surface crack are shown in Fig. 12a and b.

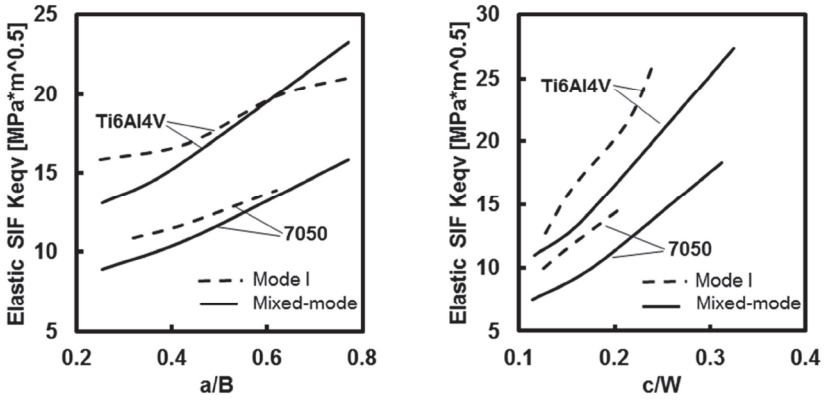

(a) (b)

Figure 12: The elastic SIFs K_{eqv} comparisons: (a) the crack front deepest point and (b) the crack front free surface.

In these figures, the crack depth *a* and crack length *c* are normalized by the SCT specimen's thickness *B=10 mm* and width *W=40 mm*. It should be noted that at the wide ranges of crack length and crack depth, the elastic SIFs K_{eqv} are significantly changed at different loading conditions, and they have increasing trends. Looking at these figures and considering changes in the SIFs along the SCT Mixed-mode specimens' crack front, differences in the crack growth rate between Mode I and Mixed-mode loading conditions are evaluated. Analysing the equivalent SIFs K_{eqv} distributions for both alloys and for all loading conditions will help for experimental results interpretation. For the further description of the fatigue fracture diagrams, the mixed mode elastic SIFs K_{eqv} as the crack size (*a*, *c)* function can be presented in the polynomial equations form.

Results and discussion

Crack growth rate interpretation

One of the main aims of the present study is the calculation of the aluminum and titanium alloys fracture resistance parameters for two surface crack propagation direction under Mode I and Mixed-mode loading, which were obtained by uniaxial tests on SCT specimens. In this section, the difference in FCG rates between surface cracks and through-thickness cracks will be presented on the fracture resistance parameters base in the literature [22].
The simple Paris law equation was used for describing the FCG rate for each load case and crack front positions:

$$da / dN = C \cdot \left(K_{eqv} \right)^m \tag{7}$$

$$dc / dN = C \cdot \left(K_{eqv} \right)^m \tag{8}$$

where da/dN is the crack extension rate based on crack depth *a* and cycle count *N*, dc/dN is the crack extension rate based on crack length *c* and cycle count *N*, *C* and *m* are material constants, K_{eqv} are elastic equivalent SIFs, obtained from Fig.12a,b. Crack growth rate diagrams as the elastic equivalent SIFs K_{eqv} function for both alloys and different loading conditions are plotted in a log–log scale on Figs. 13 and 14. As shown in these figures, for both alloys a significant crack growth rate reduction is observed in the crack front deepest point direction for Mixed-mode loading conditions. The opposite behavior is observed for Mode I loading. As shown in Fig. 14a, for titanium alloys the significant FCG rate increasing on the crack front deepest point is obtained. On the contrary, the crack growth diagrams for aluminum alloy (Fig. 13a) are barely affected by crack front positions. In any way Mixed-mode loading leads to lower crack growth rates in comparison to pure Mode I for both alloys.
Moreover, FCG rates obtained in this study are compared with those obtained using compact tension shear (CTS) specimens of the same material and sampling direction [22]. As shown in Figs. 13a and 14a, FCG rate variation is not consistent with that paper even for pure Mode I conditions. Indeed, different loading conditions leads to different crack growth curves that

are substantially different from fatigue crack growth determined on the CTS specimens. Possible reasons include the different cracks types involved that can potentially affect the FCG rate.

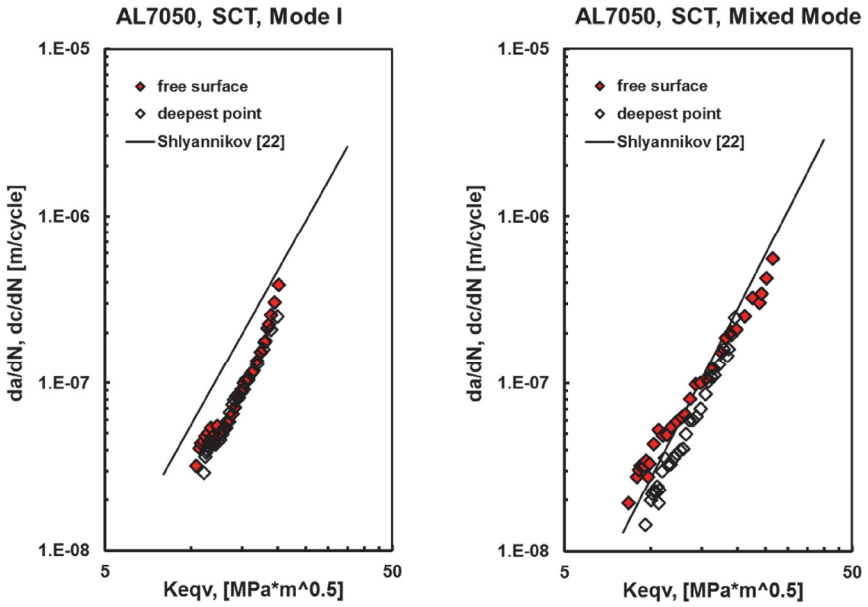

(a) (b)

Figure 13: Crack growth rate versus equivalent SIFs for aluminum alloy 7050 at (a) Mode I and (b) Mixed-mode loading conditions.

These FCG features for surface and through-thickness cracks at Mode I, and especially, at Mixed-mode loading conditions, should be taken into account in the engineering structures design and evaluation, as well as in procedure of crack propagation numerical simulation implemented in many specialized software tools, based on FEM, like e.g. FRANC3D, ZENCRACK, ADAPCRACK3D and so on.

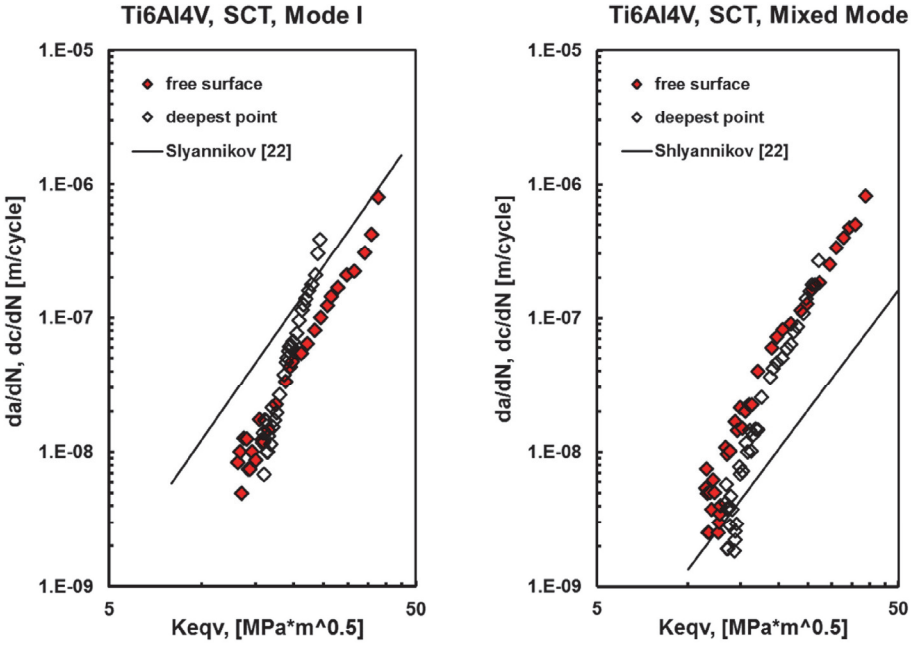

(a) (b)

Figure 14: Crack growth rate versus equivalent SIFs for titanium alloy Ti6Al4V at (a) Mode I and (b) Mixed-mode loading conditions.

Material constants *C* and *m* of Eqs. (7, 8), determined on the present research, shown in Table 3. In general, the constants *C* and *m* values, which belong to the FCG diagrams linear parts of each investigated material, are determined as a result of statistical processing of the diagrams of the tested materials.

Material	Fracture mode	(da/dN) vs elastic SIF Keqv		(dc/dN) vs elastic SIF Keqv	
		m	C	m	C
7050	Mode I	3.501	$0.683*10^{-11}$	3.724	$0.369*10^{-11}$
	Mixed-mode	3.534	$0.541*10^{-11}$	2.604	$0.879*10^{-10}$
Ti6Al4V	Mode I	8.461	$0.638*10^{-18}$	4.459	$0.653*10^{-13}$
	Mixed-mode	5.483	$0.310*10^{-14}$	4.036	$0.321*10^{-12}$

Table 3: Cyclic fracture resistance parameters for tested materials.

Conclusions

In this study, the computational and experimental results for inclined surface cracks in the modified ASTM E740 SCT specimens made of aluminum and titanium alloys were provided for 3D Mixed-mode problems. The SCT specimens with surface crack plane located orthogonal to the loading direction were considered to pure Mode I conditions realization. The experimental shape, orientation and inclination of growing surface cracks angle were determined by careful analysis of all tested SCT specimens fracture surfaces. The FEM analysis was used for SIFs calculations along crack fronts, and equivalent elastic SIF formulation was applied for crack growth rate assessment under mixed mode conditions. The fracture resistance parameters of aluminum and titanium alloys for two crack propagation directions were obtained under Mode I and Mixed-mode loading conditions. The experimental results' comparison with the fracture resistance parameters available in the literature for through-thickness cracks are presented.

Acknowledgment

The authors gratefully acknowledge the financial support of the Russian Science Foundation under the Project 19-79-10160.

References

[1] Shanyavskiy A.A. (2003). Tolerance in-service fatigue cracking of aircraft structures, Synergetics in engineering applications. Ufa, Russia.
[2] Shlyannikov V., Tumanov A., Zakharov A., Gerasimenko A. (2016). Surface flaws behavior under tension, bending and biaxial cyclic loading, International Journal of Fatigue, 92, pp. 557-576. DOI: 10.1016/j.ijfatigue.2016.05.003.
[3] Shanyavskiy A. (2011). Fatigue cracking simulation based on crack closure effects in Al-based sheet materials subjected to biaxial cyclic loads, Engineering Fracture Mechanics, 78, pp. 1516–1528. DOI: 10.1016/j.engfracmech.2011.01.019.
[4] Shlyannikov V.N., Tumanov A.V. (2011). An inclined surface crack subject to biaxial loading, Int. J. Solids Struct., 48, pp. 1778-1790. DOI: 10.1016/j.ijsolstr.2011.02.024.
[5] Ayhan A.O., Yucel U. (2011). Stress intensity factor equations for mixed-mode surface and corner cracks in finite-thickness plates subjected to tension loads, Int. J. Press. Vessel. Pip. 88, pp. 181–188. DOI: 10.1016/j.ijpvp.2011.05.009.
[6] ASTM International. E740. Standard Practice for Fracture Testing with Surface-Crack Tension Specimens.
[7] Shlyannikov V., Tumanov A., Zakharov A., Gerasimenko A. (2016). Surface flaws behavior under tension, bending and biaxial cyclic loading, Int. J. Fatigue. 92, pp. 557-576. DOI: 10.1016/j.ijfatigue.2016.05.003.
[8] Zerbst U., Kiyak Y., Madia M., Burgold A., Riedel G. (2013). Reference loads for plates with semi-elliptical surface cracks subjected to tension and bending for application within R6 type flaw assessment. Eng. Fract. Mech. 99, pp. 132-140. DOI: 10.1016/j.engfracmech.2012.11.017.
[9] Shlyannikov V.N., Tumanov A.V., Boychenko N.V. (2016). Surface crack growth rate under tension and bending in aluminum alloys and steel. Procedia Engineering. 160, pp. 5-12. DOI: 10.1016/j.proeng.2016.08.856.

[10] Forth S.C., Favrow L.H., Keat W.D., Newman J.A. (2003). Three-dimensional mixed-mode fatigue crack growth in a functionally graded titanium alloy. Eng. Fract. Mech. 70, pp. 2175-2185. DOI: 10.1016/S0013-7944(02)00237-0.
[11] Shlyannikov, V.N., Yarullin, R.R., Ishtyryakov, I. (2018). Effect of temperature on the growth of fatigue surface cracks in aluminum alloys, Theoret. Appl. Fract. Mech., 96, pp. 758–767. DOI: 10.1016/j.tafmec.2017.11.003.
[12] Slyannikov VN, Yarullin RR, Ishtyryakov IS. (2015). Surface crack growth in cylindrical hollow specimen subject to tension and torsion, Frattura ed Integrita Structurale, 33, pp. 335-344. DOI: 10.3221/IGF-ESIS.33.37.
[13] Yarullin RR, Ishtyryakov IS. (2016). Fatigue Surface Crack Growth in Aluminum Alloys under Different Temperatures, Procedia Engineering, 160, pp. 199-206. DOI: 10.1016/j.proeng.2016.08.881.
[14] Pokluda J., Slamecka K., Sandera P. (2010). Mechanism of factory-roof formation. Eng. Fract. Mech. 77, pp. 1763-1771. DOI: 10.1016/j.engfracmech.2010.03.031.
[15] Richard H.A., Schramm B., Schirmeisen N.-H. (2014). Cracks on Mixed Mode loading – Theories, experiments, simulations, International Journal of Fatigue, 62, pp. 93–103. DOI: 10.1016/j.ijfatigue.2013.06.019.
[16] Shlyannikov V.N. (2013). T-stress for crack paths in test specimens subject to mixed mode loading, Eng. Fract. Mech., 108, pp. 3–18. DOI: 10.1016/j.engfracmech.2013.03.011.
[17] Broek D. (1982) The energy principle. In: Elementary engineering fracture mechanics. Springer, Dordrecht, pp 115-141. DOI: 10.1007/978-94-009-4333-9_5.
[18] ANSYS. (2009). Theory Reference for the Mechanical APDL and Mechanical Applications. Release 12.0. Available at: http://dl.mycivil.ir/reza/ans_thry.pdf.
[19] Shlyannikov, V.N., Zakharov, A.P., Yarullin R.R. (2016). Structural integrity assessment of turbine disk on a plastic stress intensity factor basis, Int J Fatigue, 92(1), pp. 234-245. DOI: 10.1016/j.ijfatigue.2016.07.016.
[20] Shlyannikov V.N., Ishtyryakov I.S. (2019). Crack growth rate and lifetime prediction for aviation gas turbine engine compressor disk based on nonlinear fracture mechanics parameters, Theoret. Appl. Fract. Mech., 103, 102313. DOI: 10.1016/j.tafmec.2019.102313.
[21] Shlyannikov, V.N., Ishtyryakov, I.S., Tumanov, A.V. (2020). Characterization of the nonlinear fracture resistance parameters for an aviation GTE turbine disc, Fatigue Fract. Eng. Mater. Struct., 43, pp. 1-17. DOI: 10.1111/ffe.13188.
[22] Shlyannikov, V., Fedotova, D. (2021). Distinctive features of crack growth rate for assumed pure mode II conditions, Int J Fatigue, 147, 106163. DOI: 10.1016/j.ijfatigue.2021.106163.